

# Optimal Design of Eigenvalues for the Full-Spectrum Modulated Nonlinear Frequency Division Multiplexing Transmission System

Ruofan Zhang<sup>ID</sup>, Lixia Xi<sup>ID</sup>, Jiacheng Wei, Jiayun Deng, Shucheng Du, Wenbo Zhang<sup>ID</sup>, Xiaoguang Zhang<sup>ID</sup>, and Xiaosheng Xiao<sup>ID</sup>

**Abstract**—Nonlinear frequency division multiplexing (NFDM) system is an optional candidate to overcome the fiber nonlinearity limit. A full-spectrum modulated NFDM system, modulating data on combined continuous spectrum (CS) and discrete spectrum (DS) together, was proposed in recent years to improve the data rates and spectral efficiency (SE) by exploiting all the degrees of freedom offered in the nonlinear spectrum. However, the selection of discrete eigenvalues greatly affects the performance of both CS and DS. Designing appropriate eigenvalues of DS is an important issue to ensure the high SE and excellent performance of the system. In this paper, we discussed the selection principle of eigenvalues and analyzed it from multiple perspectives, 11 eigenvalues with 64-quadrature amplitude modulation (64QAM) are selected for DS. Besides optimizing the eigenvalues at the transmitter, the linear minimum mean-square estimate (LMMSE) method was used at the receiver to furtherly improve the performance of DS. Through the numerical simulation, a 113 Gb/s (SE of 2.8 bits/s/Hz) full-spectrum modulated NFDM system was set up and transmitted 1120 km distance, where the Q-factors of both CS and DS are above the hard-decision forward error correction (HD-FEC) threshold. The results provide a way to design an efficiently full-spectrum modulated NFDM system.

**Index Terms**—Nonlinear frequency division multiplexing, full-spectrum, optimal selection of eigenvalues, discrete spectrum, continuous spectrum.

## I. INTRODUCTION

NONLINEAR frequency division multiplexing (NFDM) has been intensively investigated as a potential transmission scheme to combat the fiber nonlinearity limit [1], [2],

Manuscript received 11 January 2023; revised 26 March 2023; accepted 1 April 2023. Date of publication 5 April 2023; date of current version 13 April 2023. This work was supported in part by the National Natural Science Foundation of China under Grant 62171048 and in part by the Fundamental Research funds for Central Universities under Grant 2020XD-A05-3. (*Corresponding author: Lixia Xi.*)

Ruofan Zhang, Lixia Xi, Jiacheng Wei, Jiayun Deng, Xiaoguang Zhang, and Xiaosheng Xiao are with the State Key Laboratory of Information Photonics and Optical Communications, School of Electronic Engineering, Beijing University of Posts and Telecommunications, Beijing 100876, China (e-mail: ruofanzhang@bupt.edu.cn; xilixia@bupt.edu.cn; wjc123@bupt.edu.cn; dengjy@bupt.edu.cn; xgzhang@bupt.edu.cn; xsxiao@bupt.edu.cn).

Shucheng Du is with the School of Nuclear Science & Technology, Beijing Normal University, Beijing 100875, China (e-mail: dusc@bnu.edu.cn).

Wenbo Zhang is with the School of Science, Beijing University of Posts and Telecommunications, Beijing 100876, China (e-mail: zhangwb@bupt.edu.cn).

Digital Object Identifier 10.1109/JPHOT.2023.3264479

which is the main obstacle for upgrading fiber optic communication systems. NFDM systems encode data onto the so-called nonlinear spectrum of a signal by using the nonlinear Fourier transform (NFT) [2], [3]. The nonlinear spectrum consists of the discrete spectrum (DS) and continuous spectrum (CS). The DS (solitonic components) comprises a set of points (eigenvalues) in the upper-half complex plane and their associated spectral amplitudes. “Eigenvalue communication” was firstly proposed by Hasegawa and Nyu [4], which means that information is encoded into the eigenvalue for communication over fiber channel. The CS (radiative components) is a complex-valued function of real frequencies ( $\lambda \in \mathbb{R}$ ) on the complex plane. To improve the SE and performance of NFDM systems, a lot of work and effort have been done on DS-modulated NFDM systems [5], [6], [7], [8], [9], [10] and CS-modulated NFDM systems [11], [12], [13], [14], [15], [16]. However, the achieved SE of the DS system is so far very low (less than 1 B/s/Hz) [17] and the CS system faces the problem that the performance degrades due to reduced algorithm accuracy when the launch power is high [18]. Vahid Aref proposed the first full-spectrum (FS) system with the joint modulation of DS and CS together [19], which increases data rates and SE by using all degrees of freedom offered in the nonlinear spectrum. Though promising results about data transmission encoding the information on both DS and CS have been reported recently [19], [20], [21], [22], [23], data rates and SE need to be further improved by designing and optimizing CS and DS.

In a full-spectrum NFDM system, CS and DS interact and influence each other [22]. The crosstalk between CS and DS becomes significant in practical link conditions. The length of the time-domain window is related to the parameters of CS, which constrains the selection of eigenvalues of DS. Conversely, eigenvalues of DS affect the performance of CS and DS simultaneously, so the selection of eigenvalues is very critical for FS modulated NFDM system. Although there are some related works on the study of multi-eigenvalues [5], [24], [25], [26], [27], [28], designing multi-eigenvalues of DS in the FS modulated NFDM systems is still an important issue.

In this paper, we first set the CS part to give a definite time window length, where 256 subcarriers and 16QAM modulation format are adopted. On this basis, following aspects of DS part are analyzed, including the modulation format of DS, the

selection of the real and imaginary parts of the eigenvalues, the number of eigenvalues and the spacing between the real parts of the eigenvalues. The aim is to optimize the choice of DS and ensure the good performance for FS modulated system. The selection of discrete eigenvalues is further supported by analyzing the correlation of subcarriers of CS. Finally, a 113 Gb/s FS modulated NFDM transmission system was build up by numerical simulation and the performance of the system with 1120 km transmission distance was demonstrated.

## II. THE PRINCIPLE OF FULL-SPECTRUM MODULATED NFDM SYSTEM

The propagation of the optical signal  $A(\tau, l)$  along standard single-mode fibers (SSMF) can be described by the nonlinear Schrödinger equation (NLSE) [29].

$$i \frac{\partial A(\tau, l)}{\partial l} - \frac{\beta_2}{2} \frac{\partial^2 A(\tau, l)}{\partial \tau^2} + \gamma |A(\tau, l)|^2 A(\tau, l) = -i \frac{\alpha}{2} A(\tau, l), \quad (1)$$

where  $l$  is the distance along the fiber,  $\tau$  is the time co-moving with the group velocity of the envelope,  $\beta_2$  is the group velocity dispersion coefficient,  $\gamma$  is the fiber Kerr nonlinearity coefficient, and  $\alpha$  is the attenuation coefficient. For the actual fiber channel, the loss is inevitable and Erbium-doped fiber amplifier (EDFA) is used to compensate the loss. Due to the exist of the loss term, (1) is not integrable and nonlinear Fourier transform cannot be applied [1]. To satisfy integrable conditions, the lossless path-averaged (LPA) model was proposed to model signal propagation in optical links with EDFA lumped amplifications [30]. The LPA NLSE was expressed as the following format.

$$i \frac{\partial \bar{A}(\tau, l)}{\partial l} - \frac{\beta_2}{2} \frac{\partial^2 \bar{A}(\tau, l)}{\partial \tau^2} + \gamma_1 |\bar{A}(\tau, l)|^2 \bar{A}(\tau, l) = 0, \quad (2)$$

where  $\bar{A}(\tau, l)$  and  $\gamma_1$  are detailed as follows and  $L_{\text{span}}$  is the span length.

$$\bar{A}(\tau, l) = e^{-(\alpha/2)l} A(\tau, l), \quad (3)$$

$$\gamma_1 = \gamma (1 - e^{-\alpha L_{\text{span}}}) / (\alpha L_{\text{span}}) \quad (4)$$

Introduce the following normalized parameters:

$$q(t, z) = \bar{A}(\tau, l)/A_n, z = l/L_n, t = \tau/T_n, \quad (5)$$

$$A_n = \sqrt{2/(\gamma_1 L_n)}, T_n = \sqrt{|\beta_2| L_n/2} (\beta_2 < 0) \quad (6)$$

where  $T_n$  is normalized time. Then, the normalized integrable nonlinear Schrödinger equation was got, as (7).

$$i \frac{\partial q(t, z)}{\partial z} + \frac{\partial^2 q(t, z)}{\partial t^2} + 2|q(t, z)|^2 q(t, z) = 0 \quad (7)$$

NFT maps a time-domain signal  $q(t, z)$  to its unique nonlinear spectrum by the Zakharov-Shabat problem with a boundary condition [1].

$$\frac{\partial}{\partial t} \mathbf{v} = \begin{pmatrix} -j\lambda & q(t) \\ -q^*(t) & j\lambda \end{pmatrix} \mathbf{v}, \lim_{t \rightarrow -\infty} \mathbf{v}(t, \lambda) = \begin{pmatrix} 1 \\ 0 \end{pmatrix} e^{-j\lambda t}, \quad (8)$$

TABLE I  
FIBER AND SYSTEM SIMULATION PARAMETERS

Parameters	Value
Wavelength	1550nm
Group velocity dispersion coefficient $\beta_2$	$21.67 \text{ ps}^2 \text{ km}^{-1}$
Fiber attenuation coefficient $\alpha$	$0.2 \text{ dB km}^{-1}$
Fiber nonlinearity coefficient $\gamma$	$1.27 \text{ W}^{-1} \text{ km}^{-1}$
Span length	80km
Number of span	14
EDFA noise figure	5dB
Linear bandwidth	40GHz
Number of subcarriers	256
Modulation format of CS	16QAM

where  $\mathbf{v} = (v_1, v_2)^T$  is the eigenvector of the eigenvalue  $\lambda$ . The scattering coefficients are  $a(\lambda) = \lim_{t \rightarrow +\infty} v_1(t) e^{j\lambda t}$  and  $b(\lambda) = \lim_{t \rightarrow +\infty} v_2(t) e^{-j\lambda t}$ .

The evolution of the scattering coefficients along the distance satisfies the following rules [31]:

$$a(\lambda, z) = a(\lambda, 0), b(\lambda, z) = b(\lambda, 0) \exp(4j\lambda^2 z) \quad (9)$$

The nonlinear spectrum consists of two parts, which are defined as follows:

- i) CS: the spectral amplitude  $q_c(\lambda, z) = b(\lambda, z)/a(\lambda, z)$  for real frequencies  $\lambda \in \mathbb{R}$ .
- ii) DS:  $\{\lambda_k, q_d(\lambda_k, z)\}$  where  $\lambda_k \in \Omega$ , i.e.  $a(\lambda_k, 0) = 0$ , and the spectral amplitude  $q_d(\lambda_k, z) = b(\lambda_k, z)/\left.\frac{\partial a(\lambda, z)}{\partial \lambda}\right|_{\lambda=\lambda_k}$ . The set  $\Omega$  of isolated complex values is the set of simple roots of  $a(\lambda, 0)$  with positive imaginary part, which are called eigenvalues and do not vary with transmission distance. The discrete eigenvalues denote as  $\lambda_k = \lambda_R + \lambda_I j$ .

The nonlinear spectrum satisfies the linear evolution relationship as follows:

$$q_c(\lambda, z) = q_c(\lambda, 0) \exp(4j\lambda^2 z), \quad (10)$$

$$q_d(\lambda_k, z) = q_d(\lambda_k, 0) \exp(4j\lambda_k^2 z) \quad (11)$$

For FS modulated NFDM system, both DS and CS are loaded the information and are sent to INFT together to obtain the time domain signal of FS.

## III. THE SETUP OF FS MODULATED NFDM SYSTEM

The diagram of the b-modulated full-spectrum NFDM system is shown in Fig. 1. At the transmitter module, information is modulated on the nonlinear spectra. The data was modulated on the b-coefficients of the nonlinear spectrum to mitigate the adverse effects of noise. Table I describes the parameters of the fiber loop. At the receiver side, NFT is applied to recover the nonlinear spectrum from the time-domain waveform. Specifically, the synchronization and normalization operation are first performed. Afterwards, the Ablowitz-Ladik (AL) method [3] is used to calculate the continuous b-scattering coefficient or continuous spectrum. For the discrete part, the Newton-Raphson method [3] and bi-directional layer-peeling method are used to search the discrete eigenvalues, and calculate the discrete b-scattering coefficient and discrete spectrum [32]. The phase shift operation is followed to remove the interplay of dispersion

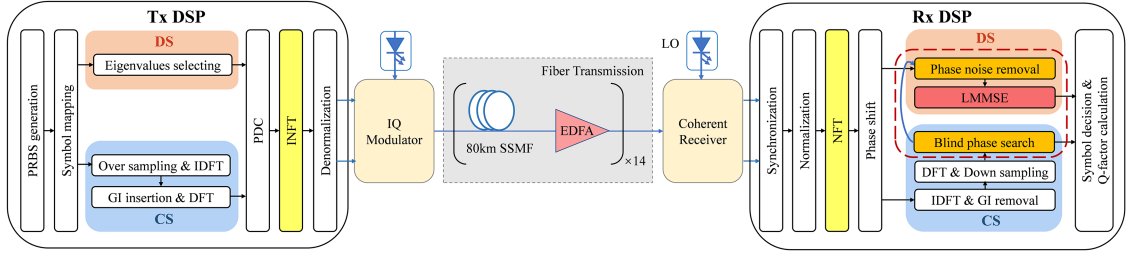


Fig. 1. Diagram of FS modulated NFDM system.

and nonlinearity. Finally, the performance is evaluated by calculating the Q-factor after the symbol decision. The Q-factor as the system performance metrics is calculated by  $Q(\text{dB}) = 20 \log_{10}[\sqrt{2}e\text{erfc}^{-1}(2\text{BER})]$ , where the bit error rate (BER) is calculated by direct error counting. It should be noted that the operations in the red dotted line box are not included in the optimization analysis of the eigenvalues selection, and are applied to the system in Section V. We first set the parameters of the CS of FS and then discuss the optimal selection of eigenvalues of the DS of FS. The parameters of the CS in the FS-modulated NFDM system are as follows.

The CS is modulated by  $N_c = 256$  orthogonal subcarriers, which are described as:

$$b_c(\lambda) = Ae^{-2j\lambda^2 z} \Gamma_b \left( \sum_{k=-N_c/2}^{N_c/2} C_k \frac{\sin(\lambda T_0/T_n + k\pi)}{\lambda T_0/T_n + k\pi} \right), \quad (12)$$

where  $\lambda \in \mathbb{R}$  and  $\lambda$  is the nonlinear frequency,  $A$  is the power control parameter,  $z$  is the normalized transmission distance,  $\Gamma_b$  is the exponential scaling in [10],  $e^{-2j\lambda^2 z}$  corresponds to the pre-dispersion compensation (PDC), and  $C_k$  is the symbol drawn from the 16QAM constellation.  $T_n = 1 \text{ ns}$  is the normalized time parameter, and  $T_0 = N_c/B = 6.4 \text{ ns}$  is the useful block duration with the system bandwidth  $B = 40 \text{ GHz}$ . To avoid the inter-symbol interference (ISI) during propagation, a guard interval (GI) of 3.2 ns is considered, resulting the total NFDM block duration  $T_1 = T_0 + GI = 9.6 \text{ ns}$  and the data rate of 106.7 Gb/s corresponding to CS.

For DS part, the factors, such as the modulation format, the real and imaginary parts of the eigenvalues, the number of eigenvalues and the spacing between the real parts of the eigenvalues, not only affect the performance of the CS, but also have an impact on the performance of the DS. Next, we will analyze these factors detailly.

#### IV. THE SELECTION PRINCIPLE OF EIGENVALUES OF DS

The principle of eigenvalue selection is to make the SE as high as possible on the premise of ensuring the performance of CS. For DS of FS, to ensure the transmission performance, the pulse component should be completely in the normalized time window before and after transmission, that is, the boundary condition of return to zero should be satisfied. Usually, the pulse containing 99.99% energy is regarded as an integrate pulse, which can be

used to calculate the pulse width and to measure whether the pulse moves out the time window.

For a b-modulation DS system, the time-domain waveform is given by [6].

$$q_d(t) = -2j\lambda_I e^{-j\angle q_d(\lambda_k)} \operatorname{sech}(2\lambda_I(t - t_0)) e^{-2j\lambda_R t} \quad (13)$$

where  $q_d(\lambda_k) = 2j\lambda_I b(\lambda_k)$ ,  $\angle q_d(\lambda_k)$  is the spectral phase,  $t_0 = \frac{1}{2\lambda_I} \ln(|b(\lambda_k)|)$  is the initial time center of the signal. After propagation with the normalized transmission distance  $z$ , the time-center of the pulse will evolve according to

$$t_0(z) = -4j\lambda_R z + \frac{1}{2\lambda_I} \ln(|b(\lambda_k)|) \quad (14)$$

##### A. Modulation Format of DS

The data rate and SE of the FS modulated system are related to the modulation format of DS, so it is important to analyze the modulation format of the DS. For the FS system, the influence of DS modulation format on CS and itself should be considered. A simple case of one eigenvalue is selected for analysis, where  $\lambda = \pi + 1j$ . The DS modulation of 128QAM, 64QAM, 16QAM, and Quadrature phase shift keying (QPSK) is considered, and the Q-factor performances of CS in these cases are compared. It can be seen from Fig. 2(a) that the performances of CS have almost no difference. On the premise of ensuring the performance of the CS, a higher-order DS modulation format is preferred to maximize SE. However, the performance of DS is very poor in the case of just one eigenvalue with 128QAM modulation format, as shown in Fig. 2(b). Therefore, 64QAM is selected for DS.

##### B. The Real and Imaginary Parts of Eigenvalues

How to select the eigenvalues? The necessary condition is that both the transmitted and received waveforms must be completely inside the time window. Furtherly, the calculation errors of NFT/INFT algorithms should be as small as possible.

The imaginary part of the eigenvalue determines the pulse energy of DS [1]. The larger imaginary part means pulse containing more energy, while calculation error will become larger for higher pulse energy. Fig. 3(a) shows the pulses (energy of CS is set to 0) with different imaginary parts of the eigenvalue ( $\lambda_R = \pi$ ). The larger the imaginary part is, the more concentrated the pulse energy is and the narrower the pulse width is. Moreover, the right boundary of the pulse corresponding to  $\lambda_I = 0.5$  does not meet the return to zero boundary condition. Considering the requirements of boundary conditions and calculation errors, we

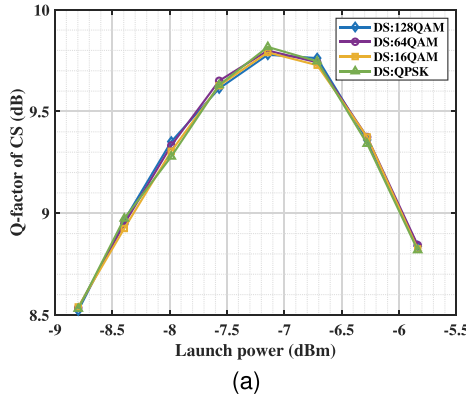


Fig. 2. Q-factor as a function of the launch power under different DS modulation formats, (a) CS, (b) DS.

choose the imaginary part as  $1j$ . On the other hand, the imaginary part  $\lambda_I$  and the magnitude of the signal  $|b(\lambda_k)|$  decide the initial position of the pulse. When  $\lambda_I = 1$  and the modulation format of DS is 64QAM, there are 9 possible values of  $|b(\lambda_k)|$ , thus resulting in 9 different pulses, as shown in Fig. 3(b). Different color lines represent symbols with different amplitudes, pulses from left to right correspond to  $|b(\lambda_k)|$  from small to large. The center positions of all transmitter pulses are located at the right side of the symmetrical axis. The initial position  $t_0$  corresponding to the leftmost pulse with the smallest amplitude is 0.25. Note that this is the case with the symbols after PDC.

According to formula (14), for a given imaginary part of the eigenvalue and modulation format, the moving direction of the pulse is related to the real part of the eigenvalue. For positive real part, the pulse will move to the left, while for the negative real part, the pulse moves to the right. As shown in Fig. 3(b), if we choose the negative real part, it is easier to move out of the window as the transmission distance increases or the window shrinks. Therefore, the energy of the pulse with the positive real part is more concentrated in the center of the window after transmission and it is appropriate to modulate positive real parts of eigenvalues.

### C. The Number and the Spacing Between the Real Parts of the Eigenvalues

In a fixed time window, the number of eigenvalues and the spacing among the real parts of the eigenvalues are constrained

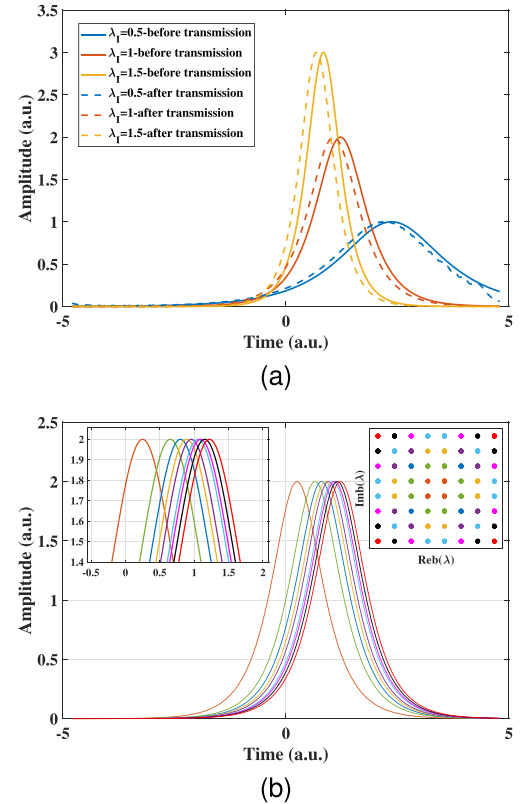


Fig. 3. (a) 1-soliton pulses with eigenvalue  $\lambda = \pi + \lambda_I j$  before and after transmitting 1120 km distance without link noise. (b) 1-soliton pulses with eigenvalue  $\lambda = \pi + 1j$  at transmitter (different colors represent different amplitudes of 64QAM symbols).

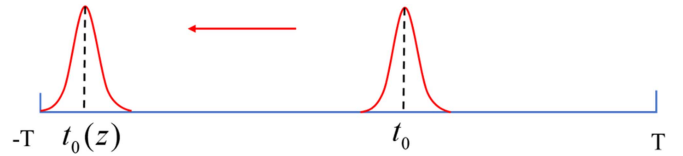


Fig. 4. Illustration of pulse propagation in a normalized time window.

each other, there exists a trade-off. The more number eigenvalues, the higher the SE, the narrower spacing between adjacent eigenvalues. However, proper spacing is required to ensure the performance. The selection principles for the number of multi-eigenvalues and the real part spacing are as follows: (i) ensure the received pulse not moving out of the time window and maintain an acceptable system performance; (ii) select as many eigenvalues within the window as possible.

According to the length of normalized time window  $[-T, T]$  and pulse moving direction, the maximum moving distance of the pulse can be calculated. Then according to the formula  $\lambda_R = \frac{t_0(z) - t_0}{-4z}$ , the maximum real value of eigenvalue  $\max(\lambda_R)$  can be obtained, as shown in Fig. 4. For the case of the real parts of eigenvalues are all positive, the relationship between the number of eigenvalues  $N$  and the spacing of the real parts of eigenvalues  $\delta$  satisfies  $N = [\max(\lambda_R)/\delta]$  (where  $[\cdot]$  indicates to take an integer).  $N$  determines the SE, and  $\delta$  affects the performance of the system.

Next, the eigenvalue selection of this system is analyzed in detail. For the window of  $[-4.8, 4.8]$  and the given pulse width,  $\max(t_0(z))$  can be calculated. According to the initial position of the pulse  $t_0 = 0.25$  and the normalized distance  $z = 0.0121$ , the maximum value of the real part of the eigenvalue is approximated as  $17.5\pi$ . The eigenvalues can be expressed as  $\lambda_n = n\delta + 1j$  and  $n = 1, 2, \dots, N$ . In this paper, we select  $\delta$  as  $0.25\pi$ ,  $0.5\pi$ ,  $\pi$  and  $1.5\pi$ , respectively. When the spacing is  $1.5\pi$  and the maximum real part is not more than  $17.5\pi$ , the maximum number of the eigenvalues is 11. Then, the performances of CS and DS at these four spacing are compared with the same number of eigenvalues of 11. For the real part spacing are  $0.25\pi$ ,  $0.5\pi$ ,  $\pi$ , and  $1.5\pi$ , the corresponding Q-factors of the CS are 6.06, 6.41, 8.85, and 7.77 respectively. Apparently, only when the spacing is  $\pi$ , the Q-factor of CS overs the HD-FEC threshold.

To furtherly analyze the spacing affecting the performance of CS, another important metric, the cross correlation of subcarriers is adopted. We compare the cross correlation of continuous spectrum subcarriers for the above-mentioned four cases. Let  $\mathbf{X} = [\mathbf{X}_1 \mathbf{X}_2 \dots \mathbf{X}_N]$  denotes the randomly chosen 16QAM data modulated on  $N_c$  subcarriers and  $\mathbf{Y} = [\mathbf{Y}_1 \mathbf{Y}_2 \dots \mathbf{Y}_N]$  denotes the received noisy data of subcarriers after NFT processing. Using the covariance matrix  $\mathbf{K}$  to describe the correlation of the subcarriers. The element of  $\mathbf{K}$  is defined as  $k_{mn} = E[(\mathbf{W}'_m - E[\mathbf{W}'_m])(\mathbf{W}'_n - E[\mathbf{W}'_n])]$ , where  $\mathbf{W} = [Re(\mathbf{Y}), Im(\mathbf{Y})]$ , and  $\mathbf{W}'$  is obtained from  $\mathbf{W}$ , that is, the real and imaginary parts of each subcarrier are arranged in sequence.  $m$  in  $k_{mn}$  represents the number of rows in  $\mathbf{K}$ , and  $n$  in  $k_{mn}$  represents the number of columns in  $\mathbf{K}$ . Both  $m$  and  $n$  are from 1 to  $2N_c$ , and the cross correlation between each subcarrier and other subcarriers is  $\sum_{m=1}^{2N_c} k_{mn} - k_{nn} - k_{ln}$  ( $n = 1, \dots, 2N_c$ ), where  $n$  indicates the index, and the real and imaginary parts of the subcarriers are arranged alternately. When  $n$  is odd,  $l = n + 1$ , it means to calculate the cross correlation between the real part of this subcarrier and other subcarriers, and when  $n$  is even,  $l = n - 1$ , it means to calculate the cross correlation between the imaginary part of this subcarrier and other subcarriers. We randomly generated 20 inputs. For each input, at the optimal power point of the CS, the corresponding NFDM symbol transmission was simulated 500 times under the influence of different random noise. The number of error symbols corresponding to each subcarrier and the cross correlation can be calculated in each input case on average, and the result is shown in Fig. 5(a) and (b). The result indicates that the eigenvalues can increase the cross correlation of nearby subcarriers, which is related to the  $\delta$ . The interference is more obvious when  $\delta$  is small, and the error symbols are concentrated in the subcarriers with strong correlation. We also observed the time-domain pulses of the FS before and after transmission with the spacing of  $\pi$  and  $1.5\pi$ , as shown in Fig. 6(a) and (b). The reason for the occurrence of the error symbols when  $\delta$  becomes larger may be that the pulse boundary does not return to zero. By comparing the number of error symbols of each subcarrier when  $\delta$  is different, finally, we choose  $\delta = \pi$ .

The Q-factors of DS with different real part of eigenvalues are shown in Fig. 7(a). With the increase of spacing, the performance

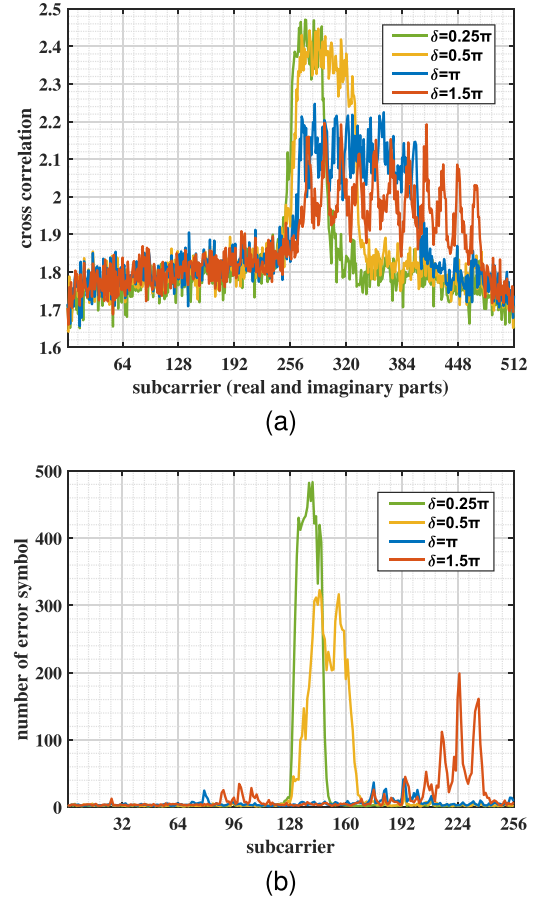


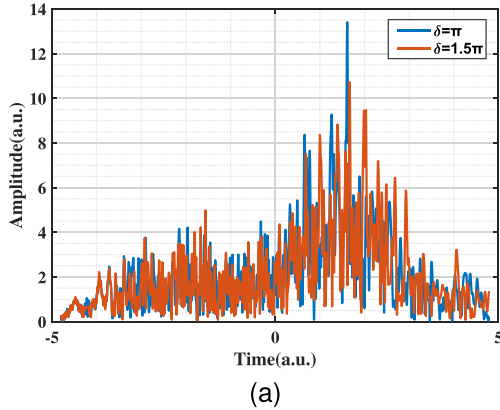
Fig. 5. (a) The cross correlation of each subcarrier with different real parts spacing of eigenvalues. (b) The average number of error symbols per subcarrier corresponding to each input.

of DS becomes better. We also observe the pulse (energy of CS is set to 0) before and after transmission with different spacing, as shown in Fig. 7(b) and (c). It is found that when the spacing is small, the right trailing of the pulse at the transmitter does not satisfy the boundary condition of return to zero. This can greatly affect the performance of DS.

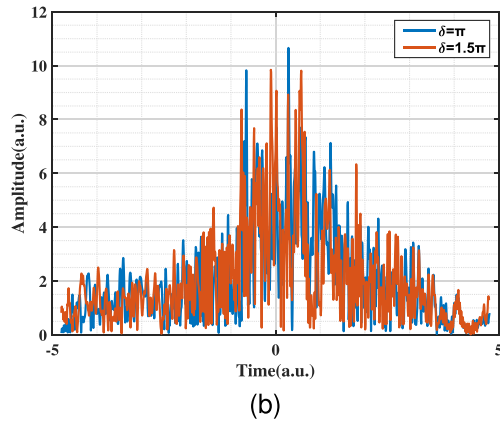
According to the above analysis, the real part spacing of eigenvalues has a great influence on the performance of both continuous and discrete spectra. Here, we choose  $\pi$  as the real part spacing of eigenvalues. Therefore, for the DS, 11 discrete eigenvalues  $\lambda_k = k\pi + 1j$ ,  $k = \{1, 2, \dots, 11\}$  are selected. The data rate of the DS achieves 6.9 Gb/s. Therefore, the optimal design of discrete eigenvalues improves the SE of the system by 6% compared to the case without discrete spectra.

## V. FURTHER OPTIMIZE AND IMPROVE SYSTEM PERFORMANCE

Now all the system parameters have been determined, and the eigenvalues have been selected optimally. We set up a FS modulated NFDM system with 1120 km transmission distance and 100 kHz lasers linewidth. To recover the phase noise of the laser, a red dotted line block is added at receiver DSP, corresponding to the system diagram in Fig. 1. The phase noise of the CS is estimated and removed by using the blind phase



(a)



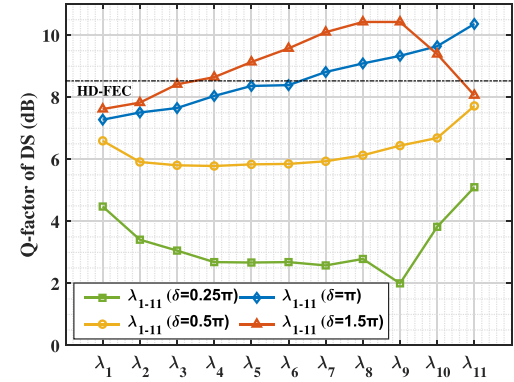
(b)

Fig. 6. The pulse of FS with  $\pi$  and  $1.5\pi$  real parts spacing of the eigenvalues, (a) at the transmitter, (b) after transmitting 1120 km distance without link noise.

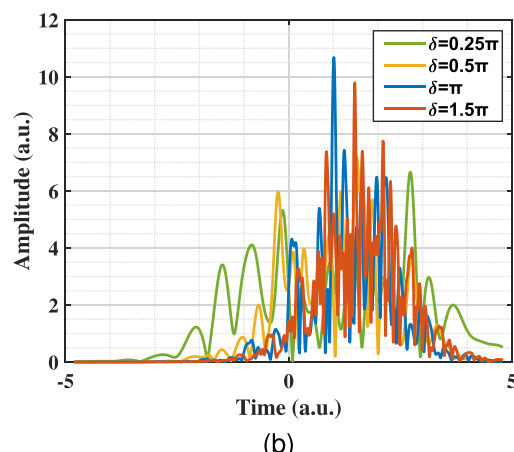
search (BPS) algorithm. And the phase noise removal (PNR) is used to remove the phase noise of DS, which is performed using the estimated results from the CS. Although the influence of phase noise is same, CS and DS have different symbol rates and the PNR method can obtain better results than BPS for DS.

To demonstrate the advantages of FS modulation, we compare it with the pure CS-modulated NFDM system. Fig. 8(a) illustrates the linear Fourier spectrum of the NFDM signal. 11 eigenvalues are visible in the linear Fourier spectrum of FS, but the occupied bandwidth does not increase. Fig. 8(b) shows the performance of the two systems. Compared with the pure CS, the Q-factor of the FS decreases by 1 dB but is still over the HD-FEC threshold and the optimum launch power increases over 4.4 dB. The launch power of full spectrum system  $P = P_c + P_d$ , where  $P_c$  represents the power of CS, and  $P_d$  represents the power of DS. According to the trace formula in [3],  $P_d$  is only determined by the number of eigenvalues and their imaginary parts. It is well known that with the increase of launch power, the traditional communication system will be more seriously affected by fiber nonlinearity. Therefore, compared with traditional communication systems such as orthogonal frequency division multiplexing (OFDM) system, the advantage of our full-spectrum modulated NFDM system to resist nonlinearity is more obvious.

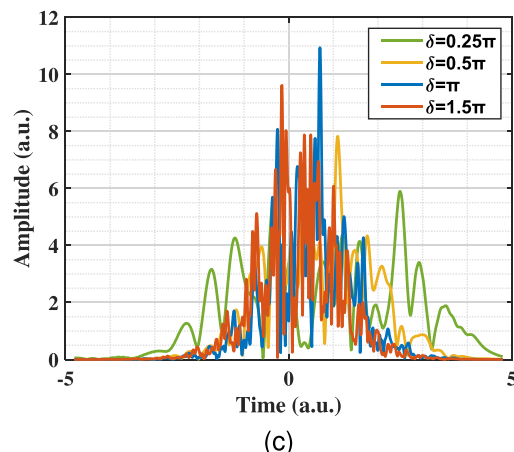
The blue line in Fig. 9 shows the Q-factor of the DS corresponding to each eigenvalue after the PNR operation at the



(a)



(b)



(c)

Fig. 7. (a) Q-factors of DS corresponding to each eigenvalue with different real parts part spacing of eigenvalues. Pulses with eigenvalues  $\lambda = \{1, 2, \dots, 11\}\delta + 1j$ , (b) at the transmitter, (c) after transmitting 1120 km distance without link noise.

optimum power point of the FS. Most of the Q-factors of the DS are lower than the HD-FEC threshold. To improve the performance of the DS, we consider the correlation between amplitude deviation  $\Delta\Gamma_b$  and phase deviation  $\Delta\theta_b$  of  $b(\lambda_k)$  and the real and imaginary parts deviation  $\Delta\lambda_R$ ,  $\Delta\lambda_I$  of  $\lambda_k$ . Because the correlation between  $\Delta\Gamma_b$  and  $\Delta\lambda_R$ , as well as between  $\Delta\theta_b$  and  $\Delta\lambda_I$ , is very small and almost negligible, Fig. 9 only shows

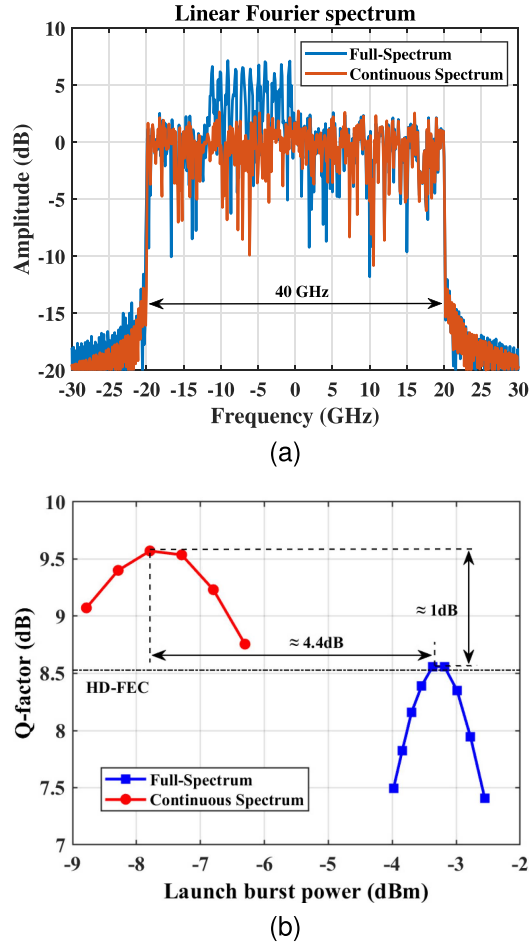


Fig. 8. (a) The Fourier spectrum of the NFDM signal. (b) The Q-factor performance of FS and pure CS system.

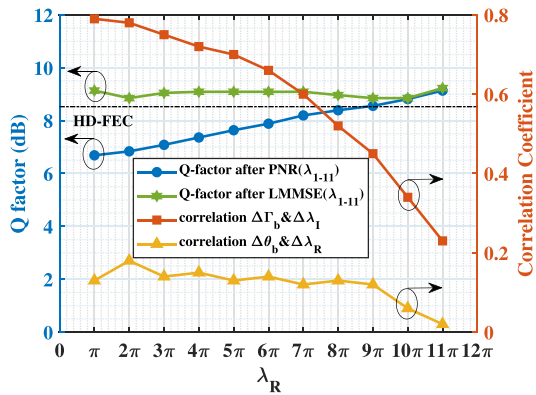


Fig. 9. The correlation between the deviation of  $b(\lambda_k)$  and the corresponding deviation of eigenvalues  $\lambda_k$ , and the Q-factor of the DS.

the results of the other two groups with correlation. One can clearly see that  $\Delta\Gamma_b$  correlates very strongly with  $\Delta\lambda_I$ , but  $\Delta\theta_b$  shows weak correlations with  $\Delta\lambda_R$ . Using their correlations, the LMMSE equalizer [8] is adopted and the Q-factor of the DS corresponding to each eigenvalue is over the HD-FEC threshold.

## VI. CONCLUSION

In this work, on the premise that the selected CS parameters has already achieve high data rate and SE, the optimal selection of eigenvalues of DS of FS is obtained by analyzing the modulation format of DS, the real and imaginary parts of the eigenvalues, the number of eigenvalues and the spacing between the real parts of the eigenvalues. The optimized design of eigenvalues further improves the SE of the system under the condition of ensuring the system performance. The capacity of FS system can be greatly increased by selecting multiple eigenvalues with high-order QAM modulation in DS and adopting large number of subcarriers in CS. In this paper, each NFDM pulse contains 256 nonlinear continuous subcarriers with 16-QAM and 11 eigenvalues with 64-QAM. Through the LMMSE equalizer, the performance of DS was furtherly improved by using the correlation between DS and the corresponding eigenvalues. The Q-factors of both CS and DS are above the HD-FEC threshold. We implemented a 113 Gb/s (spectral efficiency of 2.8 bits/s/Hz) FS modulated NFDM transmission system over 1120 km by numerical simulation. The results show a great potential for designing the high-performance FS NFDM systems.

## REFERENCES

- [1] M. I. Yousefi and F. R. Kschischang, "Information transmission using the nonlinear Fourier transform, Part I: Mathematical tools," *IEEE Trans. Inf. Theory*, vol. 60, no. 7, pp. 4312–4328, Jul. 2014.
- [2] S. K. Turitsyn, "Nonlinear Fourier transform for optical data processing and transmission: Advances and perspectives," in *Proc. IEEE Eur. Conf. Opt. Commun.*, 2018, pp. 1–3.
- [3] M. I. Yousefi and F. R. Kschischang, "Information transmission using the nonlinear Fourier transform, Part II: Numerical methods," *IEEE Trans. Inf. Theory*, vol. 60, no. 7, pp. 4329–4345, Jul. 2014.
- [4] A. Hasegawa and T. Nyu, "Eigenvalue communication," *J. Lightw. Technol.*, vol. 11, no. 3, pp. 395–399, Mar. 1993.
- [5] S. Hari, F. Kschischang, and M. Yousefi, "Multi-eigenvalue communication via the nonlinear Fourier transform," in *Proc. IEEE 27th Biennial Symp. Commun.*, 2014, pp. 92–95.
- [6] H. Buelow, V. Aref, and W. Idler, "Transmission of waveforms determined by 7 eigenvalues with PSK-modulated spectral amplitudes," in *Proc. 42nd Eur. Conf. Opt. Commun.*, 2016, pp. 1–3.
- [7] T. Gui, C. Lu, A. Lau, and P. Wai, "High-order modulation on a single discrete eigenvalue for optical communications based on nonlinear Fourier transform," *Opt. Exp.*, vol. 25, no. 17, pp. 20286–20297, 2017.
- [8] T. Gui, S. K. Lo, X. Zhou, C. Lu, and P. Wai, "4 Bits/symbol phase and amplitude modulation on a single discrete eigenvalue for nonlinear Fourier transform based transmissions," in *Proc. Opt. Fiber Commun. Conf.*, 2017, pp. 1–3.
- [9] G. Chao et al., "Alternative decoding methods for optical communications based on nonlinear Fourier transform," *J. Lightw. Technol.*, vol. 35, no. 9, pp. 1542–1550, May 2017.
- [10] A. Vasylchenkova, J. E. Prylepsky, N. B. Chichkov, and S. K. Turitsyn, "Multieigenvalue communication paired with b-modulation," in *Proc. IEEE 45th Eur. Conf. Opt. Commun.*, 2019, pp. 1–4.
- [11] X. Yangzhang, V. Aref, S. T. Le, H. Buelow, D. Lavery, and P. Bayvel, "Dual-polarization non-linear frequency-division multiplexed transmission with b-modulation," *J. Lightw. Technol.*, vol. 37, no. 6, pp. 1570–1578, Mar. 2019.
- [12] S. T. Le and H. Buelow, "64 × 0.5 Gbaud nonlinear frequency division multiplexed transmissions with high order modulation formats," *J. Lightw. Technol.*, vol. 35, no. 17, pp. 3692–3698, Sep. 2017.
- [13] S. T. Le, K. Schuh, F. Buchali, and H. Buelow, "100 Gbps b-modulated nonlinear frequency division multiplexed transmission," in *Proc. Opt. Fiber Commun. Conf.*, 2018, pp. 1–3.
- [14] S. T. Le, V. Aref, and H. Buelow, "125 Gbps pre-compensated nonlinear frequency-division multiplexed transmission," in *Proc. IEEE Eur. Conf. Opt. Commun.*, 2017, pp. 1–3.

- [15] X. Yangzhang, V. Aref, S. T. Le, H. Buelow, and P. Bayvel, “400 Gbps dual-polarisation non-linear frequency-division multiplexed transmission with b-modulation,” in *Proc. Eur. Conf. Opt. Commun.*, 2018, pp. 1–3.
- [16] S. T. Le, V. Aref, and H. Buelow, “High speed precompensated nonlinear frequency-division multiplexed transmissions,” *J. Lightw. Technol.*, vol. 36, no. 6, pp. 1296–1303, Mar. 2018.
- [17] S. T. Le, “Nonlinear frequency division multiplexing: From single polarization to dual polarization,” in *Proc. IEEE 24th OptoElectronics Commun. Conf. Int. Conf. Photon. Switching Comput.*, 2019, pp. 1–3.
- [18] M. Pankratova, A. Vasylchenkova, S. A. Derevyanko, N. B. Chichkov, and J. E. Prilepsky, “Signal-noise interaction in optical-fiber communication systems employing nonlinear frequency-division multiplexing,” *Phys. Rev. Appl.*, vol. 13, no. 5, 2020, Art. no. 054021.
- [19] V. Aref, S. T. Le, and H. Buelow, “Demonstration of fully nonlinear spectrum modulated system in the highly nonlinear optical transmission regime,” in *Proc. IEEE 42nd Eur. Conf. Opt. Commun.*, 2016, pp. 1–3.
- [20] A. Vahid, S. T. Le, and H. Buelow, “Modulation over nonlinear Fourier spectrum: Continuous and discrete spectrum,” *J. Lightw. Technol.*, vol. 36, no. 6, pp. 1289–1295, Mar. 2018.
- [21] V. Aref, S. T. Le, and H. Buelow, “Nonlinear signal multiplexing for communication beyond the Kerr nonlinearity limit,” *Nature Photon.*, vol. 11, pp. 570–576, 2017.
- [22] V. Aref, S. T. Le, and H. Buelow, “Does the cross-talk between nonlinear modes limit the performance of NFDM systems?,” in *Proc. IEEE Eur. Conf. Opt. Commun.*, 2017, pp. 1–3.
- [23] F. Da Ros et al., “Dual-polarization NFDM transmission with continuous and discrete spectral modulation,” *J. Lightw. Technol.*, vol. 37, no. 10, pp. 2335–2343, May 2019.
- [24] A. Span, V. Aref, H. Bülow, and S. T. Brink, “Time-bandwidth product perspective for nonlinear Fourier transform-based multi-eigenvalue soliton transmission,” *IEEE Trans. Commun.*, vol. 67, no. 8, pp. 5544–5557, Aug. 2019.
- [25] J. Koch, S. Li, and S. Pachnicke, “Transmission of higher order solitons created by optical multiplexing,” *J. Lightw. Technol.*, vol. 37, no. 3, pp. 933–941, Feb. 2019.
- [26] A. Span, V. Aref, H. Buelow, and S. T. Brink, “On time-bandwidth product of multi-soliton pulses,” in *Proc. IEEE Int. Symp. Inf. Theory*, 2017, pp. 61–65.
- [27] T. Kodama, T. Zuki, K. Mishina, and A. Maruta, “Hyper multi-level modulation based on optical eigenvalue multiplexing,” in *Proc. Photon. Switching Comput.*, 2018, pp. 1–3.
- [28] S. Hari, M. I. Yousefi, and F. R. Kschischang, “Multieigenvalue communication,” *J. Lightw. Technol.*, vol. 34, no. 13, pp. 3110–3117, Jul. 2016.
- [29] G. Agrawal, *Nonlinear Fiber Optics*, 5th ed. Amsterdam, The Netherlands: Elsevier, 2013.
- [30] S. T. Le, J. E. Prilepsky, and S. K. Turitsyn, “Nonlinear inverse synthesis technique for optical links with lumped amplification,” *Opt. Exp.*, vol. 23, no. 7, pp. 8317–8328, 2015.
- [31] M. J. Ablowitz and H. Segur, “Solitons and the inverse scattering transform — front matter,” in *Studies in Applied and Numerical Mathematics*. Philadelphia, PA, USA: SIAM, 1981, doi: [10.1137/1.9781611970883](https://doi.org/10.1137/1.9781611970883).
- [32] S. Hari and F. R. Kschischang, “Bi-directional algorithm for computing discrete spectral amplitudes in the NFT,” *J. Lightw. Technol.*, vol. 34, no. 15, pp. 3529–3537, Aug. 2016.